Revised Conceptual Design for the Collimator

H. Ludewig

April 1998

Collider Accelerator Department

Brookhaven National Laboratory

U.S. Department of Energy

DISCLAIMER

REVISED CONCEPTUAL DESIGN FOR THE COLLIMATOR

BNL/SNS TECHNICAL NOTE

NO. 044

H. Ludewig, A. Aronson, R. Blumberg, J. Walker,
J. Brodowski, D. Raparia, M. Todosow

April 24, 1998

ALTERNATING GRADIENT SYNCHROTRON DEPARTMENT
BROOKHAVEN NATIONAL LABORATORY
UPTON, NEW YORK 11973

Revised Conceptual Design for the Collimator

Introduction

The collimator design for the Spallation Neutron Source (SNS) has undergone several design iterations since the Conceptual Design Review (CDR) held at Oak Ridge National Laboratory (ORNL). In this technical note the revisions suggested by the reviewers at the CDR will be outlined, and their incorporation into the design discussed. The primary motivations of these changes are to reduce the cost of the collimators and to reduce the potential residual radioactive material inventory. In addition, it was suggested that more accurate techniques be used for certain aspects of the design analysis.

In the following sections the revised conceptual design, more sophisticated analysis techniques for determining stresses, and the production of secondary electrons as a result of primary proton and secondary particle interaction with the collimator tube will be discussed. Since the above work is ongoing, the next steps will be discussed in a conclusion section.

Revised Conceptual Design

The collimator conceptual design as presented at the CDR is shown in Figure 1. This design is characterized by an inner zone consisting of a layered structure of increasing blackness to protons in the direction of the beam, and shielded by iron in radial and axial directions. The shielding will reduce the leakage of secondary particles (gamma rays and neutrons). The inner structure consists of the following layered structure; borated light water, a water cooled steel particle bed, a water cooled tungsten particle bed, and borated light water. Furthermore, the collimator "bore" was assumed to be cylindrical in shape. The reviewers felt that the cost could potentially be reduced by replacing the tungsten section by an identical section consisting of copper particles. In addition, iron particles will also be considered, since this substitution can potentially result in the lowest possible cost per collimator.

A series of calculations, using the LAHET Code System (LCS) [1], were carried out to estimate the effect of these substitutions. The proton and high energy neutron (greater than 20 MeV) leakage out of the down-stream end of the collimator were used as measures of collimator performance. Substituting copper for tungsten resulted in a marginal change in the proton leakage and a slightly larger increase in neutron leakage (~ 15%). These values fall within the statistical accuracy of the calculation. In the case where iron was used instead of tungsten, both the proton and neutron leakage increased. The proton leakage increased by approximately 15% and the neutron leakage doubled. Estimates of the residual radioactivity were also made, using a combination of LCS, HMCNP4A [2], and a BNL modified version of ORIGEN [3]. It was found that the collimator using copper had approximately the same residual activity following 180 full-power days as the design based on tungsten. The design using iron instead of tungsten had a much lower inventory of radioactivity. Based on the above results it was decided to base the revised conceptual collimator design on the concept using an extended iron particle bed rather than the copper particle bed. The reasons for this choice are:

1) There is enough room in the ring structure to lengthen the collimator should it be necessary,
2) The reduction in residual radioactivity using iron will minimize the source term in the event of an accident.
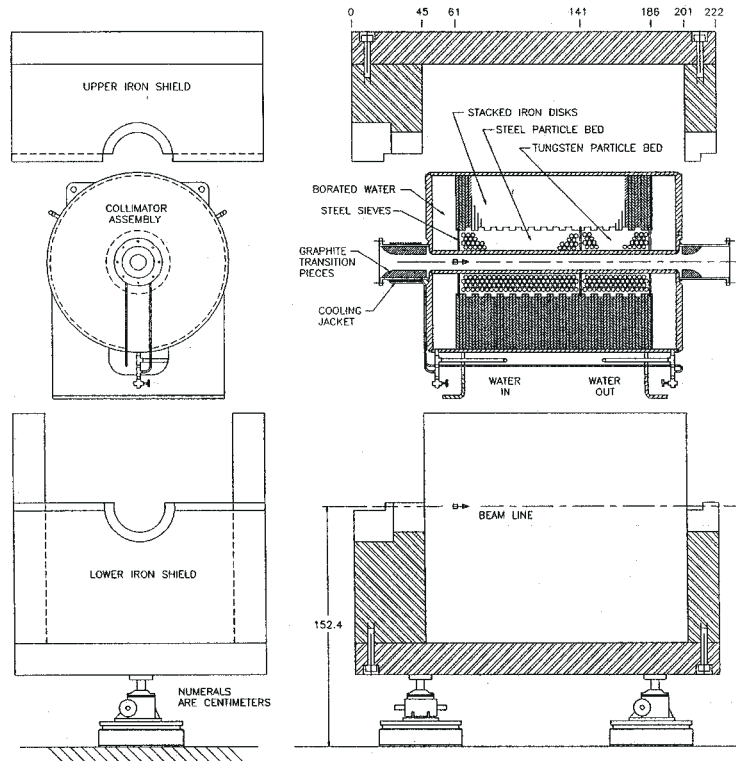
Figure 1 - Conceptual Collimator Design Presented at CDR.

The above conclusion and the collimator concept shown in Figure 1 were the starting point to develop a new configuration. Initially, the sensitivity of proton leakage out of the down-stream end to collimator length was studied. This resulted in a new conceptual design, which was used as the basis for estimating residual radioactivity, and heat deposition in the collimator tube.

A sensitivity study was carried out, using the LSC to determine the optimum length of the steel particle bed and thickness of the axial shielding. The leakage of protons and high energy neutrons out of the downstream face of the collimator was used as the measure of comparison between different configurations.

Table 1 - Proton and neutron leakage as function of particle bed length per halo proton

Bed length (cm)	Shield thickness (cm)	Proton fraction	Neutron fraction
31.1	20	1.75(-5)*	4.5(-4)
62.2	20	1.0(-6)	1.5(-4)
124.4	20	~	1.0(-5)

* 1.75(-5) = 1.75 x 10^{-5}

Based on the above results a revised collimator was configured with a particle bed length of 80 cm.

In addition, the collimator beam tube was arbitrarily assumed to be cone shaped with an included angle of $2°$. This shape is hoped to capture any additional halo particles, but the magnitude of the included angle needs to optimized. Thus in the current case primary protons will interact with the tube all the way down the axial length of the collimator, since the assumption is made that the beam is parallel to the direction of travel. The above calculations were repeated to determine the sensitivity of proton and high energy neutron leakage to the thickness of the back shield thickness.

Table 2 - Proton and neutron leakage as function of back shield thickness per halo proton

Bed length (cm)	Shield thickness (cm)	Proton fraction	Neutron fraction
80	20	3.4(-3)	4.1(-2)
80	65	1.6(-3)	9.3(-3)
96	65	1.3(-3)	7.8(-3)

The increases in leakage over the values shown in Table 1, are due to the cone shape of the inner beam tube. Secondary particles are generated axially along the tube and have a shorter distance to travel before escaping from the collimator, thus enhancing the leakage fraction. Increasing the axial shield from 20 cm to 65 cm, reduces the proton leakage by approximately a factor of two, and the neutron leakage by approximately a factor of four. Extending the particle bed into the back borated water section, effectively increasing its length from 80 cm to 96 cm, further reduces both the proton and neutron leakage by approximately 20%. Based on the above results, the proposed revised configuration for further study and analysis will have an extended back shield (65 cm thick), and a particle bed which extends into the back borated water space (96 cm long). Finally, the beam tube will be tapered with an included angle which will be location dependent. Clearly, it is seen that the currently chosen value of $2°$ is not optimum for a parallel beam. The generation of secondary particles and their subsequent transport and leakage from the collimator will be a function of this angle. The value of this angle relative to the beam angle will be the subject of a separate optimization study. The revised collimator conceptual design is shown in Figure 2. The overall component dimensions are given below in Table 3.

Table 3 - Overall component dimensions
(All dimensions in cm)

Component	Dimension
Graphite transition piece	20 (OD) x 20 (L)
Front shield	150 (OD) x 65 (L)
Collimator vessel	110 (OD) x 112 (L)
Borated water (front)	110 (OD) x ~ 10 (ID) x 16 (L)
Stainless steel particle bed	40 (OD) x ~10 (ID) x 96 (L)
Iron shield (inside vessel)	110 (OD) x 40 (ID) x 80 (L)
Radial shield (outside vessel)	150 (OD) x 110 (ID) x 112 (L)
Borated water (back)	110 (OD) x 40 (ID) x 16 (L)
Back shield	150 (OD) x 65 (L)

By adding the thickness of the axial shields to the length of the collimator vessel it is seen that the overall length of the collimator is 242 cm. The overall diameter of the collimator is seen to be 150 cm.
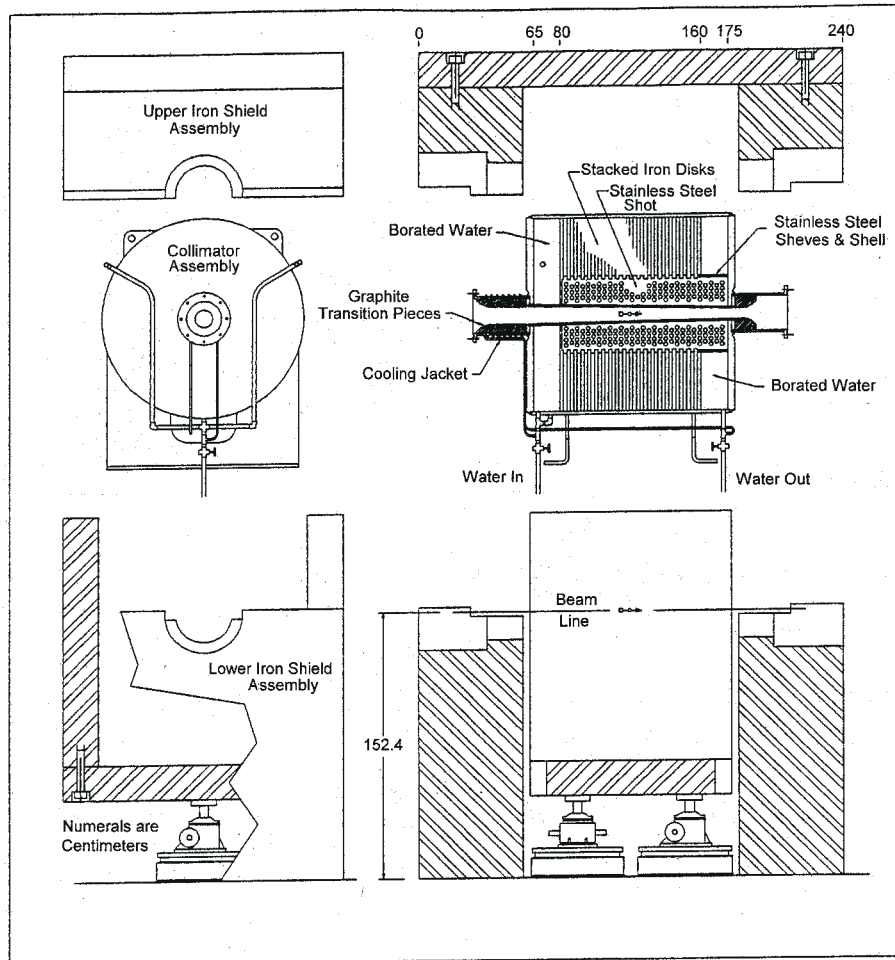
Figure 2 - Revised Conceptual Collimator Design.

The leakage of protons and neutrons per halo proton from the collimator proposed above were determined as a function of radial position and axial position. These estimates were made using the LCS and MCNP4A codes. The results were edited at various radial and axial slices. The results of these calculations for the radial distributions are given for the front and back of the collimator in Table 4. This distribution starts in the center of the collimator and proceeds to the outer radial positions. The axial distributions are shown on Table 5. These distributions start at the upstream end of the collimator and proceed to the downstream end.

Table 4 - Leakage of particles out of the front and back faces as a function of radius

Radius	Protons		Neutrons	
	Front	Back	Front	Back
2.73 - 20.0	1.9(-5)	1.2(-3)	1.4(-3)	3.2(-3)
20.0 - 30.0	~0	6.7(-5)	6.5(-4)	1.4(-3)
30.0 - 55.0	6.7(-6)	2.7(-5)	9.0(-4)	2.2(-3)
55.0 -75.0	~0	1.3(-5)	3.1(-4)	1.0(-3)

Table 5 - Leakage of particles along the axial length of the collimator

Axial position	Protons	Neutrons
0.0 - 65.0	4.7(-5)	7.5(-3)
65.0 - 81.6	6.7(-5)	1.0(-2)
81.6 - 121.6	2.7(-4)	2.8(-2)
121.6 - 161.6	2.9(-4)	1.6(-2)
161.6 - 177.6	6.7(-5)	4.4(-3)
177.6 - 226.6	1.0(-4)	7.5(-3)

The radial leakage distributions show that in the backward direction (counter to the beam direction), out of the front face, the leakage for both neutrons and protons is significantly lower than in the forward direction (direction of beam) out of the back face. Furthermore, the bulk of the leakage for both particle types is within a cylindrical area 40 cm in diameter. The axial leakage distribution shows a shallow peak for both proton and neutron leakage around the central plane of the collimator. Leakage of these particles is a strong function of the number of halo particles captured, which in turn is affected by the included angle of the collimator inner tube. The sensitivity of the above values to collimator tube angle will be determined in the next phase of this study.

The generation of radioactive nuclides (spallation products) and their decay following machine shutdown was estimated for the above collimator configuration. It was assumed that the machine operates for 180 days at full power, and the equivalent of 1 kW is deposited in the collimator for this period. The radioactivity in the collimator following this period of operation was estimated, and the radioactive nuclides were allowed to decay for 1 day, 7 days, and 30 days following shutdown. This analysis will indicate how quickly the activity can be expected to decay, and which nuclides will be active for several days and require special treatment (additional shielding due to the decay mode).

The spallation product mass distribution (residual mass estimate) was estimated using the LCS. This is similar to the fission product distribution following a nuclear fission process. The neutron energy spectrum was estimated using the MCNP4A code. A one-group cross section library was created for each spallation product nuclide by collapsing an appropriate multi-group cross section library using the neutron spectrum determined by MCNP4A. The multi-group library used for this purpose was the 63-group compilation used with the CINDER-90 code [4]. This library contains the nuclear data for 3400 nuclides. The one-group data and the nuclear decay data for the spallation products of interest are then used in an appropriately modified version of the commonly used ORIGEN code

to track the creation, destruction, and decay of the spallation products in the neutron flux while the machine is running, and following shutdown. The ORIGEN code is routinely used to calculate the activity in nuclear reactor cores due to fission products, while the reactor is operating, and following shutdown.

By sub-dividing the collimator into its components (particle bed, shields, borated water, etc.), and further dividing these into macro-zones, it is possible to determine a space dependant radioactive inventory of the collimator using the above method. The macro-zone structure shown in Figure 3 will be used in this analysis. The zones include quadrupole magnets at each end of the collimator. The position of the magnets relative to the collimator is consistent with the current ring configuration. Collimator components close to the beam entrance are sub-divided into a larger number of macro-zones, and those at the downstream end or further away from the primary beam are treated as individual blocks. In this manner spatially varying neutron energy spectra can be accommodated.
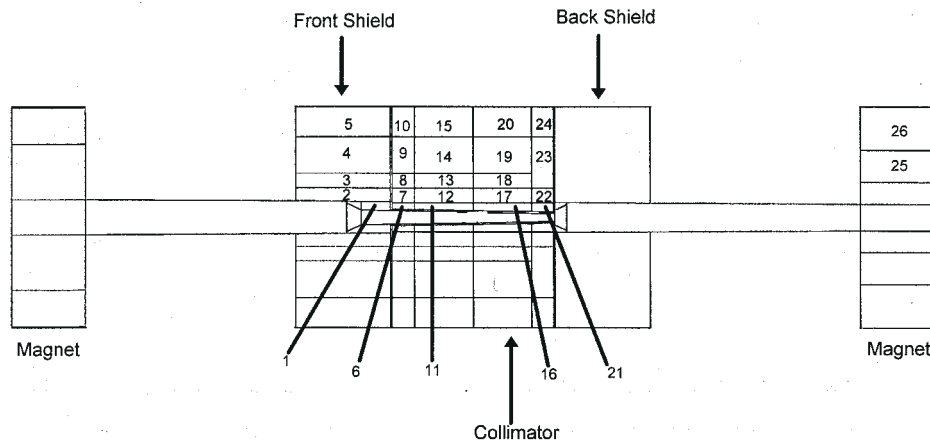

Figure 3 - Macro-zone Structure used in Activation Analysis.

Table 6 - Collimator component activation
(curies)
(Following 180 full power days assuming 1 kW is deposited in the collimator)

Cell number/description	0 days	1 day	7 days	30 days
1/Graphite transition piece	15.15	3.04	2.82	2.09
2/Front shield	10.97	8.66	7.23	5.16
3/Front shield	4.03	3.18	2.65	1.90
4/Front shield	3.38	2.67	2.22	1.59
5/Front shield	1.01	0.79	0.66	0.48
6/Borated water	3.46	0.29	0.27	0.20
7/Borated water	1.85	0.14	0.13	0.10
8/Borated water	0.68	0.05	0.04	0.03
9/Borated water	0.57	0.04	0.03	0.02
10/Radial shield	1.39	1.0	0.88	0.70

Table 6 - CONTINUED

Cell number/description	0 days	1 day	7 days	30 days
11/Particle bed	29.68	19.15	15.76	10.76
12/Particle bed	27.5	18.31	15.49	11.28
13/Internal shield	18.98	13.33	11.44	8.61
14/Internal shield	16.86	12.0	10.39	7.98
15/Radial shield	3.73	2.7	2.35	1.82
16/Particle bed	6.62	4.35	3.65	2.62
17/Particle bed	8.06	5.44	4.65	3.47
18/Internal shield	7.62	5.40	4.65	3.54
19/Internal shield	8.60	6.13	5.29	4.06
20/Radial shield	2.12	1.59	1.36	1.03
21/Particle bed	1.23	0.81	0.68	0.50
22/Particle bed	1.26	0.85	0.72	0.53
23/Borated water	0.55	0.40	0.35	0.27
24/Radial shield	8.33	5.98	5.12	3.83
25/Q-P copper	5.01	1.85	1.07	0.77
26/Q-P iron	0.23	0.17	0.15	0.11

The above results indicate that the bulk of the activity will be due to activation of components internal to the collimator. It will thus be contained within the collimator. Only the cooling water passes out of the collimator to an intermediate heat exchanger. In the event of an accident scenario which results in a non-catastrophic collimator vessel failure (for example cracks, or point failures) only that activity associated with the coolant would contribute to the source term.

The above calculations track several hundred nuclides in any given chain, and thus the major contributors to the radioactivity in any given zone can be determined. It is found that a relatively small number of nuclides contribute the bulk of the radioactivity in any component. The following are the major contributors by material type:

1) Graphite - Graphite is used in the transition pieces, and is part of the collimator structure. The major contributors to the activation of graphite are C-11 and Be-7. C-11 decays within an hour and the long term activity of graphite is controlled by Be-7, which has a 54 day half-life and decays with a 0.477 MeV gamma ray.

2) Cooling water - Cooling water is activated in the inlet plenum, particle bed, and outlet plenum. The major contributors to the activation of the cooling water are O-15, N-16, N-13, C-11, Be-7, and B-12. The most active nuclide is C-11, which decays rapidly, and the long term activity is controlled by Be-7. In view of the fact that the cooling water will have to be passed through an intermediate heat exchanger the piping and heat exchanger will have to be shielded by either lead or some high "Z" material to prevent the decay gamma ray from the Be-7 from irradiating the surroundings. The amount of tritium generated in the cooling water is very small for the operating scenario assumed above. However, this will also be contained in the cooling system, but its decay beta should not affect the surroundings.

3) Iron - Iron is found in the particle beds, and axial, and radial shields. The major contributors to the activation of iron under these operating conditions are Mn-51, Mn-52, Mn-54, Mn-56, Mn-57, Fe-52, Fe-53, Fe-55, Fe-59, Cr-49, Cr-51, Cr-55, V-47, V-48, V-49, V-52, V-53, Sc-43, Sc-44, Sc-46, Sc-47, Sc-48, Ti-45, K-42, and Co-56. Most of these nuclides have relatively long half-lives, and thus the activity of iron containing components does not decay rapidly, only the titanium and potassium isotopes decay within the first day. However, since the iron containing components are all part of the collimator structure, this activity is not expected to affect the operation and maintenance of the machine. Activation of the radial and axial shields will have to be considered more carefully, since the decay gamma rays may affect maintenance staff, and in this case a movable shield may be necessary. These components are self-shielding and a more detailed gamma ray transport analysis will be necessary to determine what if any movable shielding is required.

4) Copper - Copper is a material used in the construction of magnets at either end of the collimator. In addition, magnet maintenance may require personnel to approach and handle magnet components. The major contributors to the activation of copper are Cu-62, Cu-64, Cu-66, Fe-55, Fe-59, Mn-54, and Mn-56. The activation of copper components is primarily controlled by Cu-64, which decays within one day. The remaining activity is long lived, but the levels are comparatively low.

Heat transfer and stress analysis

In this section results of a more sophisticated heat transfer and stress analysis will be presented than those presented at the CDR. An integrated analysis of the temperature profile, resulting thermal stresses, and stresses due to the imposed mechanical loads will be carried out. This analysis will limit itself to the collimator beam tube, since the remainder of the collimator components are essentially non-load bearing. Furthermore, any stress related failure of any of the collimator internals should not compromise its operation. However, a failure of the collimator beam tube would cause a shutdown of the entire facility. Thus, the stress levels in the beam tube should be acceptably low to ensure a long reliable operating life.

The heat deposition in the collimator tube due to primary proton beam irradiation, and due to secondary particles (neutrons and photons) was estimated using the LAHET and MCNP codes. These values were then used in a heat conduction calculation, with the appropriate boundary conditions to estimate the temperature distribution within the beam tube. The boundary condition consists of no heat removal on the inside (machine vacuum) of the beam tube, and a finite heat transfer coefficient on the outside (cooled by cooling water) of the beam tube. Finally, the thermal stress due to the temperature gradients can be estimated. In the latter calculation the beam tube is assumed to be attached to the collimator end plates which extend approximately half-way to the outside vessel wall. The boundary condition at this point is assumed to be "clamped", which will introduce an unphysical bending stress at that radius. However, the stresses in the beam tube itself should be accurate, and give an indication of the stress levels due to operation. The primary thermal stress is compressive due to thermal expansion of the beam tube relative to the remainder of the collimator structure. In addition a mechanical stress component was estimated due to operating the collimator at a pressure of 50 psi. This pressure is required to ensure adequate coolant flow, and prevent coolant boiling in the event of a large fraction of the beam being dumped at a particular spot

on the beam tube. The estimates of the temperature distribution and the subsequent stress levels were determined using the ALGOR code [5]. This code carries out the desired integrated thermal-stress analysis, described above.

The results of these calculations are shown on Figures 4 - 6. Figure 4 is an illustration of the heat deposition as a function of axial position along the beam tube. It is seen that the highest heat deposition occurs at the inlet end of the collimator, and it falls off with distance along the beam tube. The values shown on Figure 4 include a safety factor of 5, to account for any uncertainties in the heat deposition estimates. The resulting temperature distribution is shown on Figure 5. The thermal gradients are seen to be quite modest, and are not too different from those determined at the time of the CDR. Finally, the combined thermal and mechanical stresses are shown on Figure 6. The highest values (~ 7600 psi) are seen to be located in the radial zone away from the beam tube and caused by the "clamped" boundary condition. The estimated operating stress occurs at the leading edge of the tube and has a magnitude of approximately 5000 psi. This stress level is quite modest, and should make it possible to design a collimator which will operate reliably. This analysis is based on steady state operation of the machine. In reality the heating will be cyclic, consistent with the operating cycle of the machine. In the analysis to be carried out in the next phase the cyclic nature of the stress will be included. In the ring and High Energy Beam Transport (HEBT) the cyclic nature of the thermal stresses will have a relatively long period. The beam intensity in the ring builds up over several hundred LINAC pulses before being extracted and transported to the target in a pulse which is approximately 1 μs in length. In the HEBT the pulses are 1 ms long and are synchronous with the LINAC operating mode. The time structure of the heat deposition in these two components is slow enough that thermal-mechanical enhancement of the thermal stress is not expected. However, in the Ring to Target Beam Transport (RTBT), which connects the ring to the target, the time structure is the same as for the target itself. It is thus expected that enhancement of the thermal stresses associated with collimators in this line will occur. A detailed thermal stress analysis with the appropriate enhancement will be carried out in the next phase of the design.
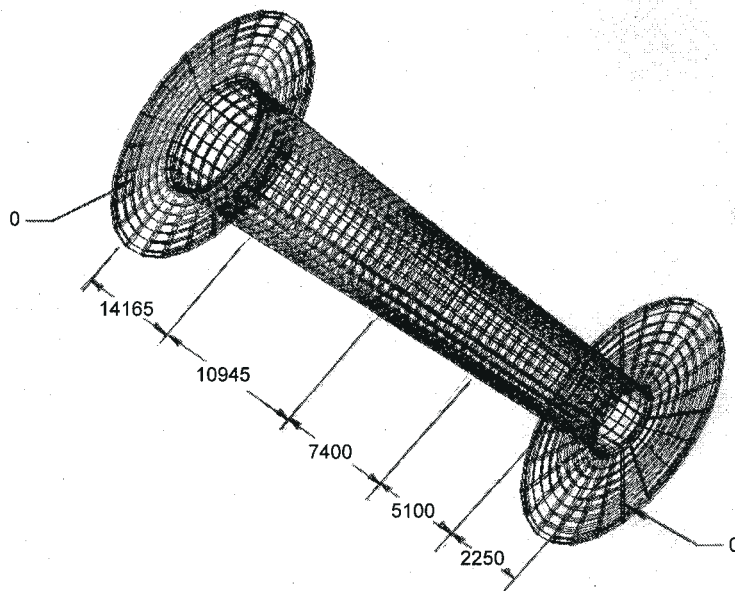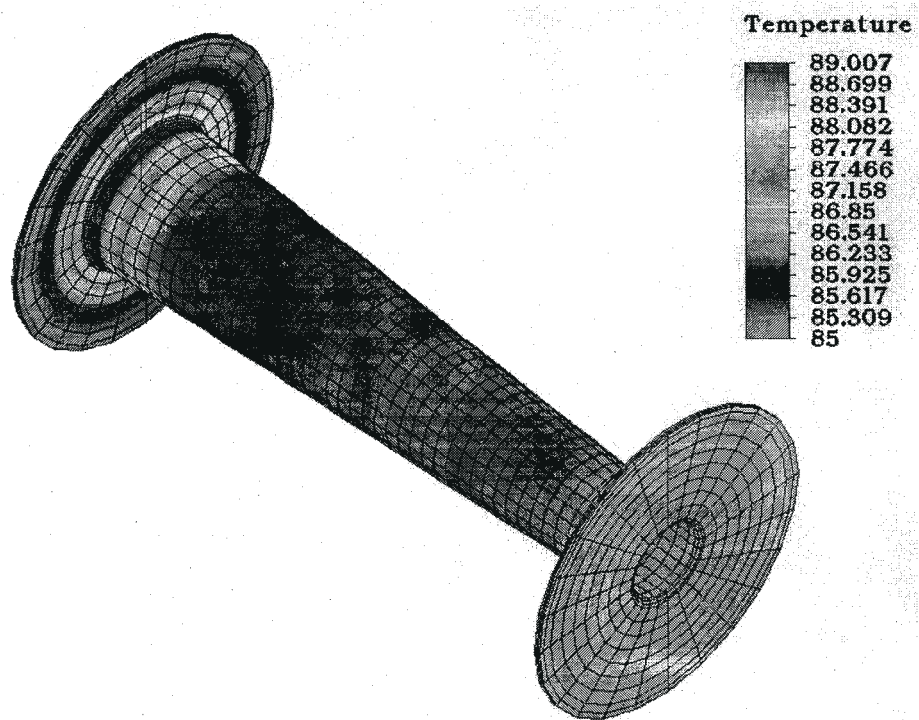

Figure 4 - Heat Deposition (W/m^3).

Temperature
89.007
88.699
88.391
88.082
87.774
87.466
87.158
86.85
86.541
86.233
85.925
85.617
85.309
85

Figure 5 - Temperature Distribution (°F).

Von Mises
7049.9
6525.9
6001.9
5477.8
4953.8
4429.8
3905.7
3381.7
2857.7
2333.7
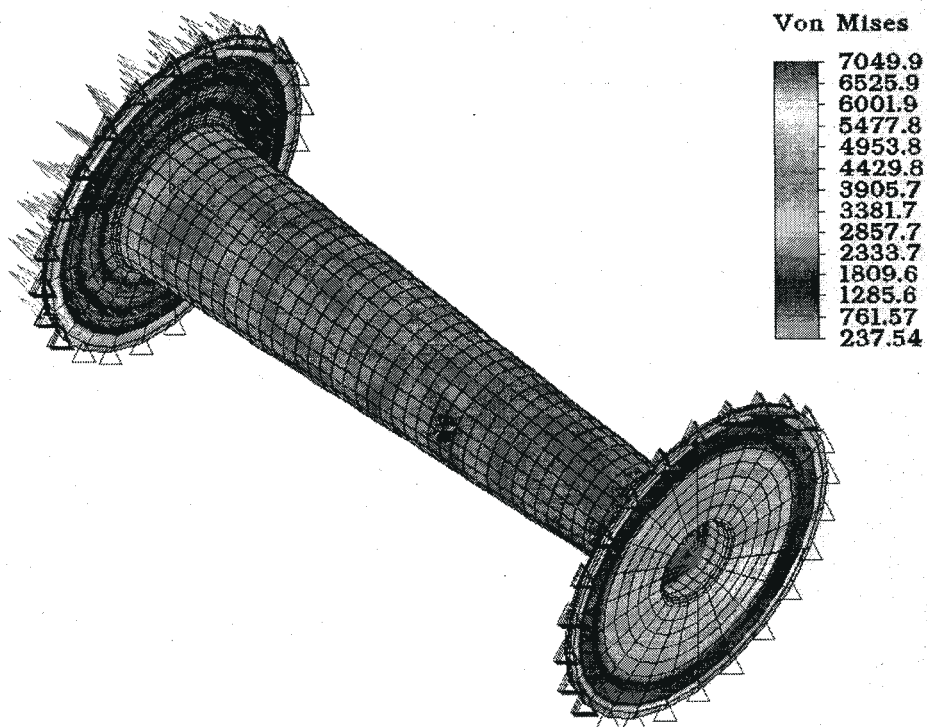1809.6
1285.6
761.57
237.54

Figure 6 - Total Static Stress (psi).

Production of Secondary Electrons in the Collimators

The production of secondary electrons due to the interaction of the primary protons and the secondary particles with the steel beam tube will be estimated using two different methods. The existence of these electrons is thought to degrade the performance of the ring. It is therefore important to estimate the number of electrons which can potentially leak into the beam tube. In addition, the energy and angular distribution of the electrons is of interest. If the number of electrons leaking into the beam tube is deemed to be too high, then mitigating features must be included in the collimator design. In the remainder of this section the two methods of determining the electron population will be described, the results from using one of the methods will be presented, and a mitigating strategy will be outlined.

The first method used to estimate the number and distribution in both energy and angle of the electrons entering the beam tube as a function of lost proton is based on a special purpose code. This code is based on the Monte Carlo method, and tracks the incoming protons which hit the collimator. The electrons produced by these protons in knock-on collisions are estimated. The probability of an electron being produced in a spatial increment Δz within an energy interval Emin to Emax is computed using the Bhabba formula. Electron angles are chosen at random from a Rutherford distribution and the corresponding energy is obtained from elastic scattering kinematics. Electrons are tracked using direction cosines and energy loss is computed from tabulated values of dE/dx. Random Coulomb scattering angles are obtained from a Moliere distribution. Electrons exiting the collimator edge are sorted in energy and angle bins. The second method of estimating the production of secondary electrons and their subsequent leakage into the beam tube will be made using the revised LAHET code MCNPX [6]. This code is based on a combination of the LAHET and MCNP codes. The production and transport of all primary and secondary particles (including electrons) will be carried out simultaneously in this code. Results obtained using the special purpose code will be presented below.

The results of this analysis are presented on Figure 7 - 9. Figure 7 shows the number of electrons leaking into the beam tube as a function of included angle of the collimator tube. It is seen that this value varies from 0.25 to 2.0 depending on the magnitude of the included angle. A large increase in the number of electrons entering the beam tube occurs when the included angle exceeds the proton beam profile at that particular location (-7.82 mrad). It is thus suggested that the collimator beam tube profile follow the local beam profile as closely as possible in order to minimize the production of secondary electrons and presumably other secondary particles. Figure 8 shows the variation of the leakage electron energy distribution integrated over all angles. This is a monotonically decreasing function with increasing energy. The largest number of electrons occur at the lowest energies. This result will be significant in designing a mitigation scheme. Finally, Figure 9 shows the angular distribution of electrons leaving the beam tube surface integrated over all the energies. It is seen that there is a maximum in the distribution at approximately one radian, which corresponds to approximately $60°$ from the surface of the beam tube. The results outlined in the above work correspond to one configuration and several collimator tube included angles. The calculations will be repeated using the combined version of LAHET and MCNP before a final decision will be made to change the design.
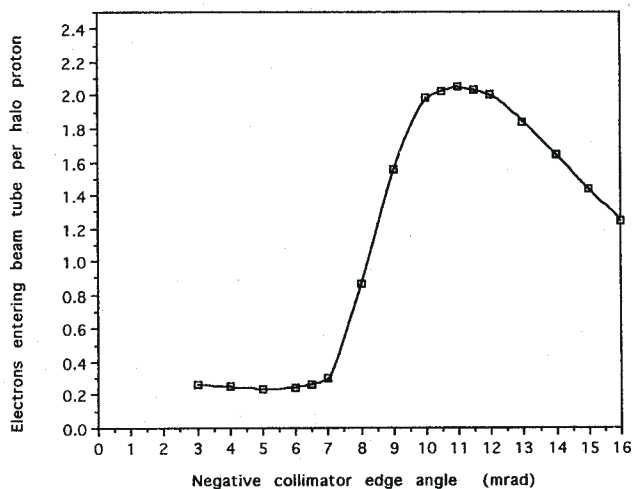
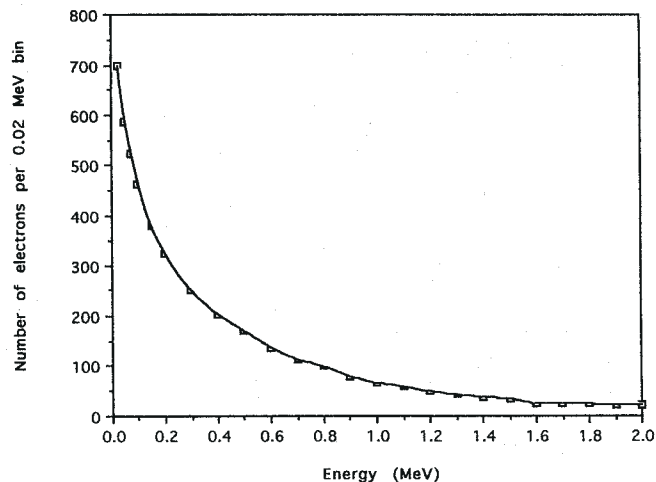Figure 7 - Number of Electron per Captured
Proton Entering Collimator Beam Tube.

Figure 8 - Energy Spectrum of Electrons
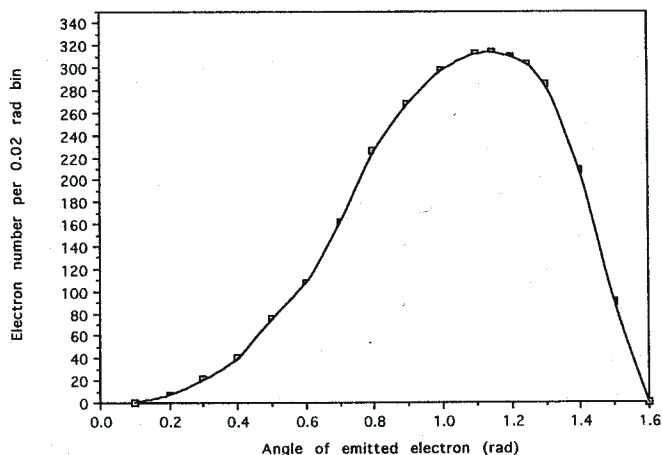Entering Collimator Beam Tube.

Figure 9 - Angular Distribution of Electron Entering Collimator Beam Tube.

In order to minimize the effect of secondary electrons on the circulating proton beam in the ring, or in the RTBT it might be necessary to remove the electrons as they are produced by an appropriate electric or magnetic field. Preliminary estimates of two such mitigating techniques have been investigated, and are described below. Both techniques involve electric fields applied by including conductors inside the collimator beam tube. In one case a quadru-pole field was used, and in the second case a di-pole field was used. These fields were created by appropriately charged conductors placed within the beam tube. Detailed design configurations have not been worked out for these arrangements. At this stage only the electric field profiles and possible electron orbits in these fields have been estimated for various field strengths and electron energies. The field profiles were estimated using the SAMION code [7].

A quadru-pole field was created by having four conductors all with the same positive voltage. In this way the field has four cusp shaped valleys surrounding the conductors. It was thought that electrons would be attracted to the conductors and thus be removed from the beam tube. However, those

electrons which emerge from the beam tube at the locations where the cusp shapes meet the tube travel across the diameter of the tube in an unimpeded manner. This field configuration is thus not the optimum solution for removing electrons. A di-pole field was produced by having four alternately charged conductors placed around the inside diameter of the beam tube. In this manner a di-pole field can be created, and preliminary results indicate that regardless of where the electrons are created on the surface of the beam tube they will be swept out. The possibility that the di-pole field will affect the proton beam is very small, since its magnitude will be relatively low. This effect will be addressed in more detail as the design matures and whether there is a need for removing the secondary electrons becomes clearer.

Conclusions

The following conclusions can be drawn from the above preliminary study:

1) Replacing the tungsten portion of the collimator with stainless steel and increasing the length of the axial shield by 45 cm resulted in a revised collimator design which should be less expensive than the preliminary design presented at the CDR, have a lower inventory of radioactive materials at the end of life, and perform equally well at stopping the halo protons and the secondary particles. This design needs to be carried a step further to include transient effects and variations in the collimator beam tube included cone angle.

2) The more sophisticated stress analysis indicated that the steady state stresses in the beam tube, which is the most crucial component of the collimator, are modest and should not pose any undue mechanical challenges to the operation of the collimator. A more sophisticated transient stress analysis of the collimator beam tubes associated with the collimators placed in the RTBT will have to be carried out. This analysis will determine the magnitude of the thermal stress enhancement due to thermal-mechanical shocks, which could occur in this location since the proton pulse length is 1 μs.

3) The production of secondary electrons and their mitigation by applied electric fields was investigated. The primary conclusion from this study was that to minimize the production of secondary electrons the profile of the collimator beam tube should follow the local beam profile. The applicability of this conclusion to other secondary particle (neutrons, photons, and protons) production will be investigated in the next phase of the study. Preliminary results indicate that a di-pole electric field is potentially the best at sweeping out secondary electrons.

References

[1] R.E. Prael and H. Lichtenstein, 'User Guide to LCS: The LAHET Code System", Los Alamos National Laboratory, Los Alamos, NM. LA-UR-89-3014 (1989).

[2] MCNP-A General Monte Carlo N-Particle Transport Code Version 4A, J.F. Breismeister, ed., Los Alamos National Laboratory, Los Alamos, NM. LA-12625-M (1993).

[3] A.G. Croff, "ORIGEN2 - A Revised and Updated Version of the Oak Ridge Isotope Generation and Depletion Code", Oak Ridge National Laboratory, Oak Ridge, TN. (1977).

[4] W.B. Wilson, "Accelerator Transmutation Studies at Los Alamos with LAHET, MCNP, and CINDER-90", Los Alamos National Laboratory, Los Alamos, NM. LA-UR-93-3080 (1993).

[5] "ALGOR - A Finite Element Analysis Code", Algor Interactive Systems Inc., 260 Alpha Drive Pittsburgh, PA. 15238. (1990).

[6] H. Grady. Hughes, et al. "The MCNP/LCS Merger Project", Proc. Topical Meeting on Nuclear App. Of Accelerator Technology, p.213, Albuquerque, NM. (1997).

[7] D.A. Dahl and J.E. Delmore,"The SIMION PC/PS2 User's Manual - Version 4.0", Idaho National Engineering Laboratory, EG&G Idaho, Idaho Falls, ID. EGG-CS-7233 (1986).